First spacecraft demise workshop - Test case description and results

Martin Spel, Vincent Rivola, Bastien Plazolles

FIRST SPACECRAFT DEMISE WORKSHOP – TEST CASE DESCRIPTION AND RESULTS

Spel Martin [(1)], Rivola Vincent [(1)], Plazolles Bastien [(1),(2)]

[(1)] R.Tech, Parc Technologique Cap Delta, 09340Verniolle, France
Email : martin.spel@rtech.fr
[(2)] CNRS, LAAS, 7 avenue du colonel Roche, F-31400 Toulouse, France
Université de Toulouse, LAAS, F-31400 Toulouse France

ABSTRACT

In order to assess the ground risk of spacecraft operations that should comply with national and international space law regulations, a large number of spacecraft demise tools have recently been developed. In order to treat the complexity of the physical processes involved, different approaches are followed, from low fidelity "object oriented" tools, to higher fidelity "spacecraft oriented" tools.
The lack of experimental data and the multidisciplinary aspect of the process make the validation and verification a challenging task.
Many codes are based on simplified methods, often a heritage of research performed in the '60s for nuclear missile re-entry. However at that time, the uncertainty margins applied were such to favour a safe entry. For spacecraft risk assessment the uncertainty margins however should be the opposite. Todays computational means allow techniques such as computational fluid dynamics and thermal analysis codes to verify the models used in current tools.
In the current paper we present an initiative to enlarge the available data for validation and verification of spacecraft demise software. A collaborative initiative in the form of a workshop, common practice in the aeronautical industry (drag prediction workshop, SPICES, etc), is proposed. The initiative allows comparing between different tools and to assess the uncertainties between different codes and different disciplines for incorporation by a statistical approach.

The various disciplines involved have been separated in three groups: integration, where we compare between different codes the complete process of entry; thermal, where we study the thermal time evolutions for imposed heat fluxes, and aerothermal, where we study the heat fluxes and aerodynamic coefficients for a fixed reentry condition.
At later stages those disciplines could be extended by, for example, ablation or flight mechanics test cases.

The present paper describes the proposed test cases for the different disciplines, and presents a comparison of the main results obtained by the different participants to the first spacecraft demise workshop.

1. TEST CASE DESCRIPTION

Indeed, it is very important to notice that there are a lot of different disciplines included in the simulation of a debris reentry. For each of them, models are used to simplify simulations and reduce computation times. Thus the first goal should be to try to validate each discipline independently. This is the reason why these test cases are divided in three categories:

- Aerothermodynamics models validation cases: this part is directed towards the validation of the aerothermodynamics models themselves. This includes for example the validation of aerodynamic formulae used in rarefied and continuum regimes by comparing them to CFD simulations for example or to wind tunnel tests when available.
- Thermal cases: this will be the same objective as for aerothermodynamics models, i.e. comparing thermal formulae used in debris simulation tools and more advanced numerical simulations or eventually wind tunnel tests if available.
- Integration simulation cases: this part will focus on complete trajectory comparisons between the different codes and eventually with some reconstructed data from past debris reentries. The main objective of this part is to show how the differences in the modeling impact the global parameters (such as demise altitude, impact energy, impact position) of a debris re-entry.

1.1. Aerothermodynamics test cases

In order to cover simple and more complex aerodynamic effects such as shock-shock interaction for example, it has been decided to use two shapes for the comparisons.

Hollow Cylinder

The first shape is a hollow cylinder defined by three dimensions presented in Figure 1:

- L1: Length of the cylinder
- L2: External diameter of the cylinder
- L3: Thickness of the cylinder

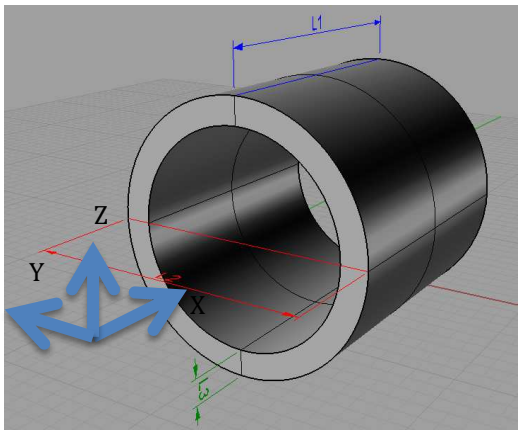

Figure 1: Definition of the studied cylinder

For the computation of aerodynamic coefficients, L_{ref} is chosen equal to $\sqrt{L1 * L2}$, S_{ref} shall be equal to 1 m^2, and the CoG shall be equal to he center of the cylinder. The reference frame is presented in Figure 2.

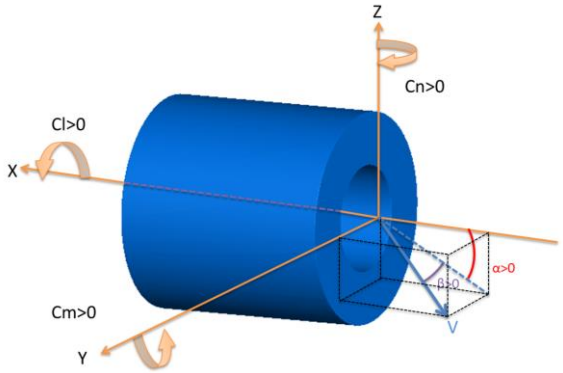

Figure 2:Inclination angles and momentum around axis

Cube

The second shape is a cube and so it is defined by only one dimension L. The reference length is chosen as L and the reference surface as $1m^2$ with the CoG at the center of the cube.

For each of the shapes a set of flow conditions has been defined, presented in Table 1, Table ***2***,Table ***3*** andTable ***4***. While in the detailed test cases description both perfect gas and non-equilibrium modeling are described, in the current paper we only describe the conditions for which a large number of institutes have participated: a Mach 9 continuum case with perfect gas assumption and a Mach 24 case in the transitional regime.

Mach	9	[-]
Speed	2.89E+003	[m/s]
Temperature	256.26	[K]
Pressure	272.72	[Pa]
Density	3.71E-003	[kg/m^3]
Re/m	6.56E+005	[m^{-1}]
Wall Temperature	700	[K]
Chemistry	Perfect gas	N.A.

Table 1: Mach 9 continuum free stream conditions

Case N°	Shape	L1 (m)	L2 (m)	L3 (m)	Mach	Angle of Attack (°)	Sideslip (°)
M001	Cylinder	1.0	1.0	0.25	9	0	0
M002	Cylinder	1.0	1.0	0.25	9	45	0
M003	Cylinder	1.0	1.0	0.25	9	90	0
M004	Box	1.0	1.0	1.0	9	0	0
M005	Box	1.0	1.0	1.0	9	45	0
M006	Box	1.0	1.0	1.0	9	45	45

Table 2: geometrical definition of cases M001 to M006

Mach	24.64	[-]
Speed	7364	[m/s]
Temperature	222	[K]
Pressure	0.00749787	[Pa]
Density	$1.18e^{-07}$	[kg/m^3]
Mass fraction N2	1	[-]
Mass fraction O2	0.0	[-]
Wall Temperature	200	[K]

Table 3: Transitional regime free stream conditions

Case N°	Shape	L1 (m)	L2 (m)	L3 (m)	Angle of Attack (°)	Sideslip (°)
X007	Cylinder	1.0	1.0	0.1	0	0
X008	Cylinder	1.0	1.0	0.5	0	0
X009	Cylinder	1.0	1.0	0.25	0	0
X010	Cylinder	1.0	1.0	0.1	45	0
X011	Cylinder	1.0	1.0	0.5	45	0
X012	Cylinder	1.0	1.0	0.25	45	0
X013	Cylinder	1.0	1.0	0.1	90	0
X014	Cylinder	1.0	1.0	0.5	90	0
X015	Cylinder	1.0	1.0	0.25	90	0

Table 4: geometrical definition of cases X007 to X015

1.2. Thermal

The objective of the thermal test cases is to validate thermodynamic (heat conduction, radiation) and ablation models used in the different debris simulation tools.

Two test cases have been identified:

- a solid sphere with uniform heat flux Boundary Conditions (BC)
- a solid sphere with axisymmetric heat flux BC

The sphere has a diameter of 1m and is composed of AA7075 with the following properties:

- Thermal conductivity: 130 W/m-K
- Specific heat capacity: 1012.35 J/kg/K
- Density: 2 787 kg/m^3
- Emissivity: 0.1

The initial temperature is imposed at 200 K after which a fixed power of 400kW is applied to the sphere.
For the first test case this power is uniformly distributed over the sphere (constant heat flux).
In the second case the net flux is expressed as:
$F = F_{Stag} * cos\theta * cos\varphi$
F_{stag} being the flux at the stagnation point in the direction of the X axis, θ the angle in the xOz plane and φ the angle in the xOy plane as defined in Figure 3. The angles are defined positive in the forward direction.

The flux at the stagnation point is equal to: $\boldsymbol{F_{stag} = \frac{400\ kW}{\pi * 0.5^2} \sim 509.296\ kW/m^2}$

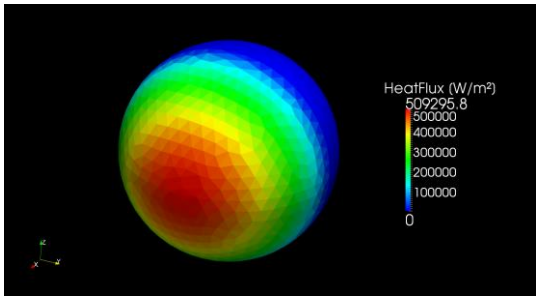

Figure 3: imposed heat flux distribution on sphere

1.3. Integration.

A total of 12 test cases is proposed, the first 8 are supposedly not demising. The last 4 are supposed to reach the melting temperatures and to eventually demise.

The entry points for the twelve test cases are defined in the Keplerian coordinate system as presented in Table 5.

	Case 1-8	Case 9-12
Semi major axis [km]	6139.7329559249	6104.1211743857
Eccentricity	0.0728268039	0.0618885792
Apogee altitude	208.7336239044	103.7601011331
Perigee altitude	-685.5406320546	-651.7906723617
Perigee argument	145.7054889438	172.3940541048
Inclination angle	45	45
Azimuth angle	45	45
RAAN	99.9064731143	99.9064709751
True anomaly	-145.7054889438	-172.3940540568
Date	2012-01-01, 00h00 UTC.	2012-01-01, 00h00 UTC.

Table 5: Entry point parameters

The description of the integration test cases is given in Table 6 and the properties of the material used in Table 7**Erreur ! Source du renvoi introuvable.**. For all test cases, the atmospheric model used for the simulations is the US Standard Atmosphere 1976.

Case N°	Shape	Width/ Diam. (m)	Length (m)	Height (m)	Mass (kg)	Thickness (mm)	Material
1	Sphere	1.0			247.2	30.0	AA7075
2	Sphere	1.0			393.6	30.0	Ti-6Al-4V
3	Cylinder	1.0	1.0		370.8	30.0	AA7075
4	Cylinder	1.0	1.0		590.4	30.0	Ti-6Al-4V
5	Box	1.0	1.0	1.0	472.2	30.0	AA7075
6	Box	1.0	1.0	1.0	751.7	30.0	Ti-6Al-4V
7	Plate	1.0	1.0		86.6	30.0	AA7075
8	Plate	1.0	1.0		133.1	30.0	Ti-6Al-4V
9	Sphere	1.0			34.7	4.0	AA7075
10	Cylinder	1.0	1.0		52.1	4.0	AA7075
11	Box	0.3	0.3	0.3	17.9	13.0	AA7075
12	Plate	0.5	0.5		10.5	15.0	AA7075

Table 6: Integration test cases description

Name	Density [kg/m^3]	Heat of fusion [J/kg]	Melting Temp. [K]	ε	Cp [J/kg/K]
AA7075	2 787	376 788	830.0	0.141	1012.35
TI-6Al-4V	4 437	393 559	1 943.0	0.302	807.5

Table 7: Material Properties

2. TEST CASE RESULTS OVERVIEW

In the current paragraph we present the comparison of the various participations to the three types of test cases.

2.1. Aerothermal

A total of 11 participants have contributed to the aerothermodynamics test cases, 6 in the continuum regime, and 5 in the transitional regime. Table 8 gives an overview of the different participants and codes used. Since both high fidelity codes (CFD and DSMC) and simplified methods have been used, we can either inter-compare the high fidelity methods in order to have an idea of the dispersion in the results, or compare high fidelity methods with simplified method in order to evaluate the precision and possible restrictions in the simplified methods.
The CFD codes are all well known to the CFD community, and most of them have been developed for non-destructive re-entry applications. While the test cases are geometrically simple, very complex flow physics occurs. First of all, the sharp angles cause attached shock waves, which are not often encountered on non-destructive re-entry cases that are typically blunt bodies (capsules, lifting body, sphere-cone configurations). Secondly, for the hollow cylinder, a very complex flow physics is observed inside and in the wake of the cylinder, as can be seen in Figure 4 .

Each participant has used different meshes. The DLR Tau code [7] has applied a grid adaptation strategy in order to capture the high gradients present in the various cases. Only the participants with highly refined meshes capture all flow gradients. For example in Figure 4 the Mach disk in the wake is only captured in the axi-symmetric MISTRAL computation and the OpenFOAM computation. In the 3D MISTRAL computation the mesh was too coarse to capture this flow phenomenon. It should be noted that capturing such a flow feature is very interesting from a scientific point of view, but that it does not influence the global parameters of interest for the demise process of the object (aerodynamic coefficient, global heat transfer). Note also that excellent agreement is obtained between the two codes in terms of position of this Mach disk. It has also been noted that the shock stand off distance is perfectly matching between all contributors. Inside the cylinder a first separation zone occurs, causing an oblique shock. At the interaction of the oblique shock and the boundary layer a secondary separation occurs, causing both a reflected shock and a second reattachment shock.

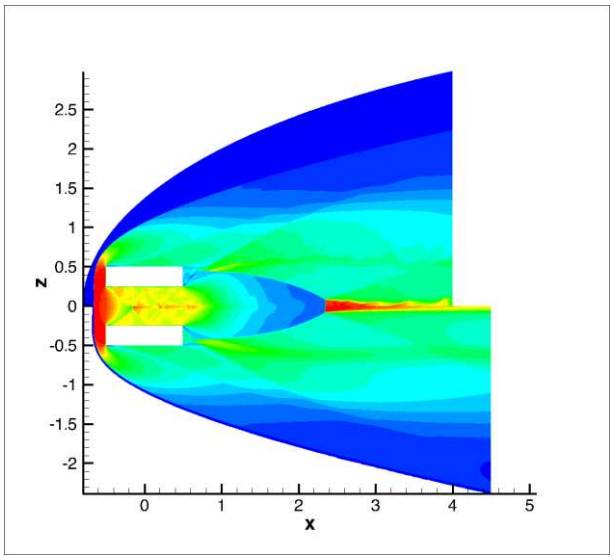

Figure 4: temperature field case 1 MISTRAL (up) and OpenFOAM (down)

Code	Contributor	Type of code
ANITA	Fluid Gravity	CFD
DsmcFoam	R.Tech	DSMC
DsmcFoamStrath	Strathclyde University	DSMC
Mistral-DSMC	R.Tech	DSMC
Mistral-CFD	R.Tech	CFD
OpenFOAM (rhoCentralFoam)	Strathclyde University	CFD
Pampero	R.Tech	Simplified method
SAM	Fluid Gravity	Simplified method
SMILE	ITAM	DSMC
SU2	R.Tech	CFD
TAU	DLR	CFD

Table 8: Aerothermodynamics contributors overview

This process is repeated once more further downstream within the cylinder.

In Figure 5 and Figure 6 the comparisons between the axial and normal forces are shown. Excellent agreement can be seen between the different CFD codes. The simplified methods both use a modified Newton method for the pressure distribution, causing a constant pressure coefficient on flat surfaces. Also those methods cannot predict any of the complex flow phenomena such as shock wave boundary layer interactions, separations and friction forces. In Figure 7 the pressure coefficients are shown for the three CFD contributions and the two simplified model contributions to case 2 (cylinder at 45° AoA). It can be seen that the TAU solution captures extremely well the gradients on the shock impingement inside the cylinder due to its grid adaptation strategy. The ANITA code [5] uses a mesh 8 times coarser than the MISTRAL computations, causing a somewhat more diffuse pressure and heat flux distribution. The simplified methods impose zero-pressure if the vector between the incoming flow and the surface normal is shadowed by another surface.

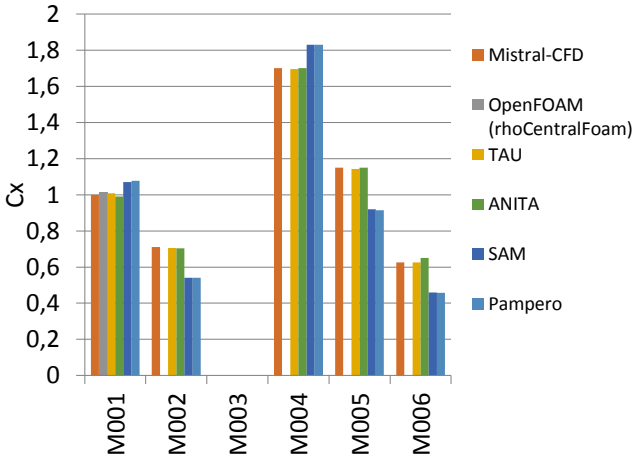

Figure 5: Axial force coefficient for Mandatory Cases

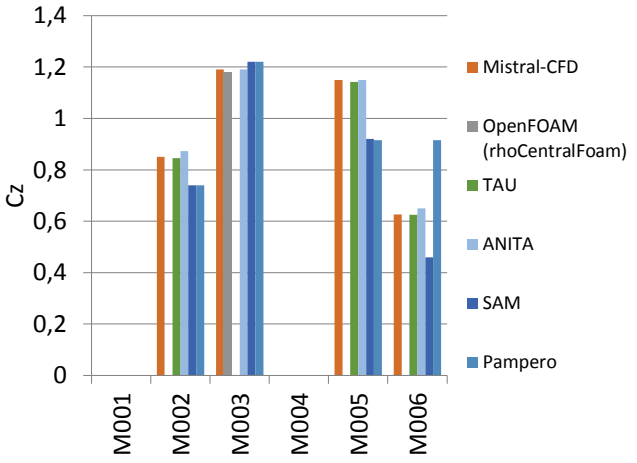

Figure 6: Normal force coefficient for Mandatory Cases

In the CFD solutions we see that in those zones the pressures are far from being negligible. On the windward side cylinder reasonable agreement is observed between CFD and simplified methods. This can also been seen in the resulting normal force for case M003 being close to the CFD solution.
For the box case at 0° AoA the simplified methods over-predict the axial force. This is due to the fact that the modified Newtonian assigns a constant pressure on the full surface, while in the CFD the pressure tends to decrease due to the acceleration of the flow around the edges as can be seen in Figure 8.

*Figure **9*** shows reasonably good agreement between the CFD results of the global heating rates (surface integral of the local heating rates). The ANITA results are only on a medium level mesh, which explains some of the dispersions. Between the MISTRAL, OpenFOAM and TAU results we observe a maximum dispersion of +/- 5%.

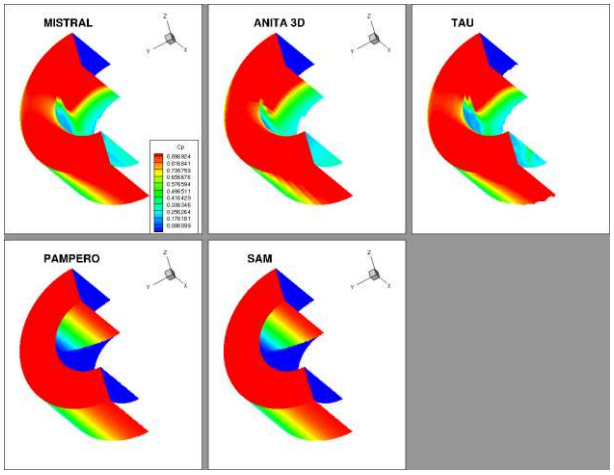

Figure 7: pressure coefficient for case M002: hollow cylinder at 45° AoA

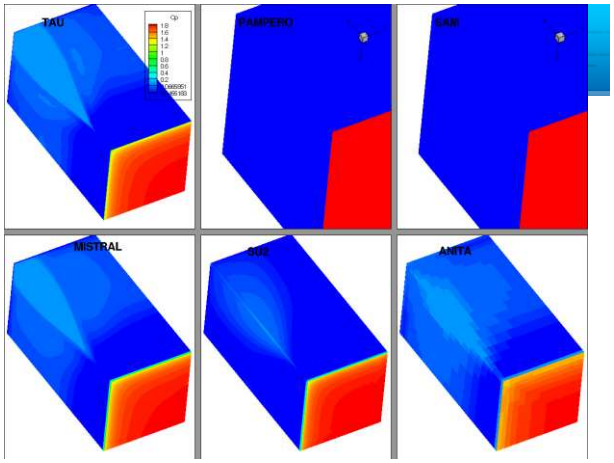

Figure 8: pressure coefficient for case M004

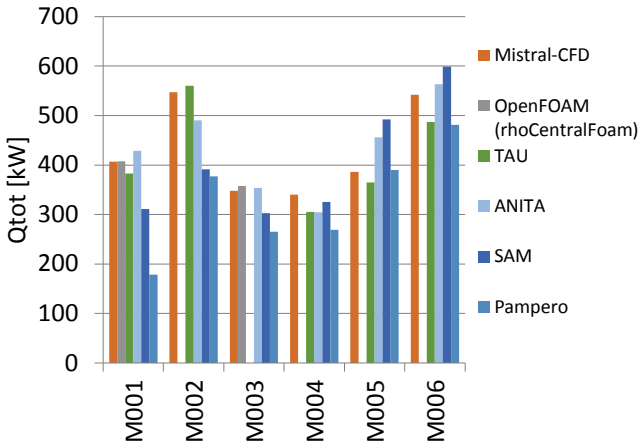

Figure 9: Surface integral of heat flux in kW for Mandatory Cases

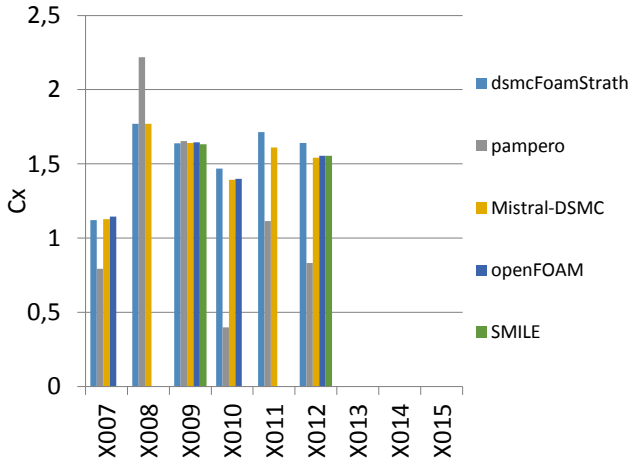

Figure 10: Axial force coefficient for Optional Cases

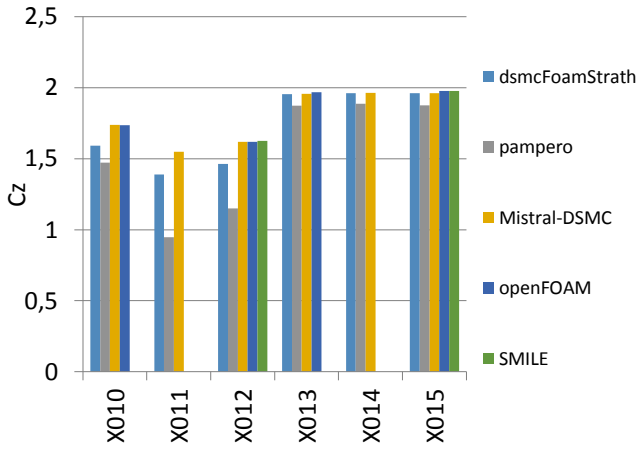

Figure 11: Normal force for Optional Cases

Regarding the optional cases in the rarefied regime an excellent agreement is observed for both the

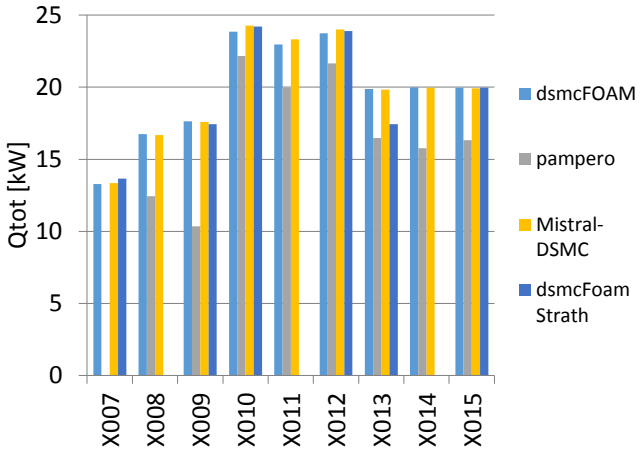

Figure 12: Surface integral of heat flux in kW for Optional Cases

aerodynamic coefficients and the global heating rates between the different DSMC codes. The simplified method in Pampero [6] seems to underpredict consistently the heating rates and shows poor results for the aerodynamic coefficients for some of the optional cases.

2.2. Thermal

Since only one contributor (CNES) participated to this test case combined with a lack of space, the analysis is postponed to a moment where multiple participations are available.

2.3. Integration

A total of 4 participants have contributed to the integration test cases, **Erreur ! Source du renvoi introuvable.** gives an overview of the different participants and codes used.

Code	Contributor	Type of code
Debrisk	R.Tech	Object Oriented
DEBRIS	DEIMOS	Object Oriented
SAM	Belstead Research	Spacecraft Oriented
SESAM	HTG	Object Oriented

Table 9: Integration contributors overview

DEBRISK: is an object-oriented code developed by CNES, for the assessment of casualty area. In DEBRISK the spacecraft is an assembly of a parent object (a cylinder or a sphere) with optional solar panels that will demise at a critical altitude and release children objects (spheres, cylinders, boxes and plates). The flight dynamic is a 3 Degree of Freedom (DoF) trajectory propagated via Sirius library, considering gravitational and aerodynamic forces. The thermal model takes into account convective, oxidation and radiation heat transfer. A lumped mass model is used for the heating model and the ablation is uniformly applied over the surface once the melting temperature is reached [3].

DEBRIS: is an in-house tool of the DEIMOS company, within the Planetary Entry Toolbox. DEBRIS is an object-oriented code. The main objectives of DEBRIS are: the footprint estimation, the analysis of debris survivability, the risk analysis and re-contact analyses. In DEBRIS, the fragmentation of the spacecraft is modelled as a single event based on trajectory parameters (e.g. thermos-mechanical loads). After the breakup of the spacecraft, the debris are treated as independent objects. Dynamics and thermal analysis are decoupled. The flight dynamic is a 3 DoF trajectory propagated with a variable step Runge-Kutta integrator considering gravitation and aerodynamic forces. Aerothermodynamic model consider stagnation heat flux based on Detra-Kemp-Riddel model and FMF bridging. Wall temperature and mass loss are based on lumped model [2].

SAM (Spacecraft Aerothermal Model): in an object-oriented code developed by Fluid Gravity and Belstead Research. For the workshop, SAM results are provided with two configurations: SAM aerodynamic and heating shape factors used as baseline, or SAM aerodynamic with SESAM heating factors [1]. More results are available on the Belstead Research website: http://www.belstead.com/scdw2015/index.html

SESAM (Spacecraft Entry Survival Analysis): is an object oriented code developed by HTG for ESA. Like for DEBRISK, in SESAM a spacecraft is a parent container object with optional solar panels, containing child objects of pre-defined shapes: sphere, cylinder, box, plate. Parent object and solar panels break-off at a predefined altitude. The flight dynamic is a 3 DoF trajectory propagated with a Runge-Kutta integrator considering gravitational and aerodynamic forces. The thermal model considers lumped mass heat storage and re-radiation. Ablation is uniform over the surface of the object once melting temperature is reached [4].

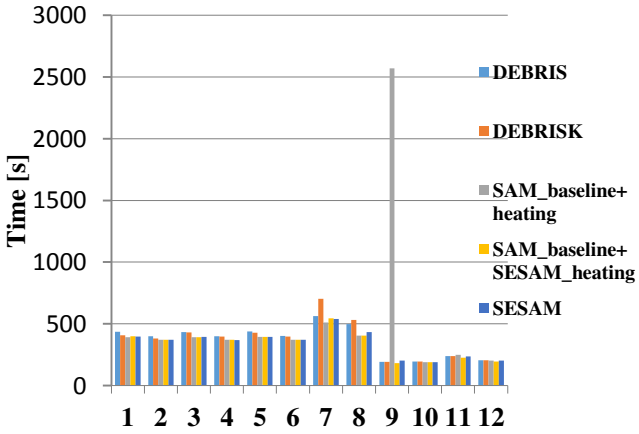

Figure 13: Atmospheric re-entry duration in seconds of

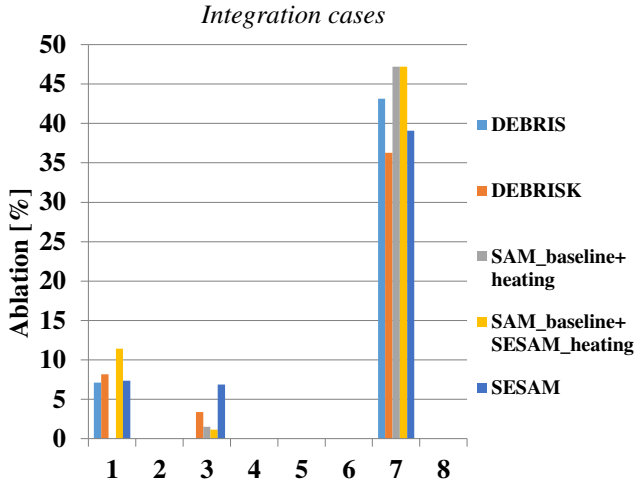

Figure 14: Ablation rate of the non-demising Integration cases

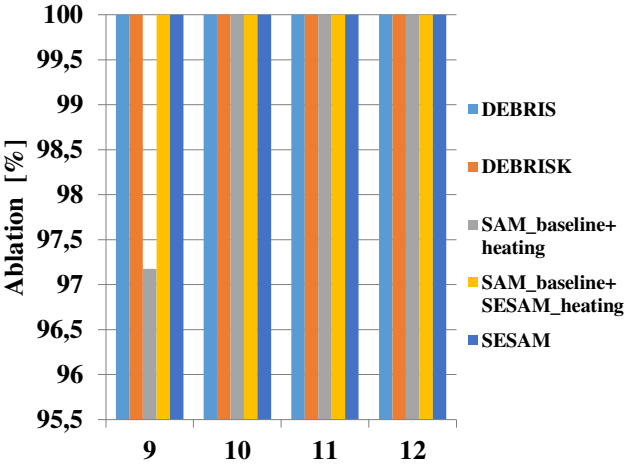

Figure 15: Ablation rate of the demising Integration cases

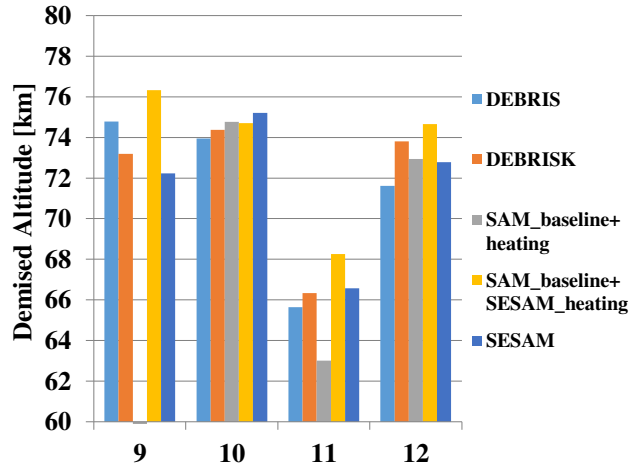

Figure 16: Demised altitude in km

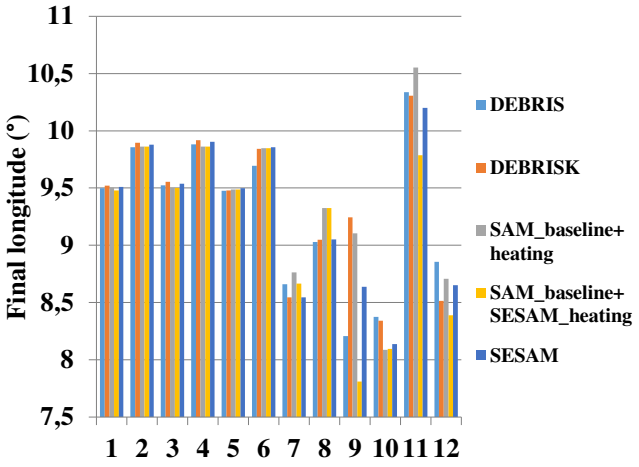

Figure 17: Longitude of the impact of demised point

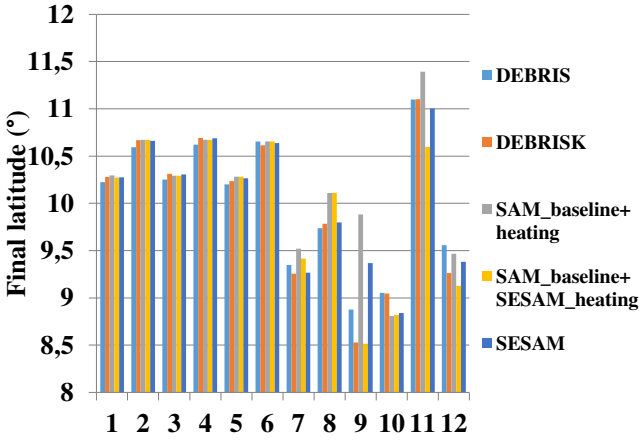

Figure 18: Latitude of the impact or demised point

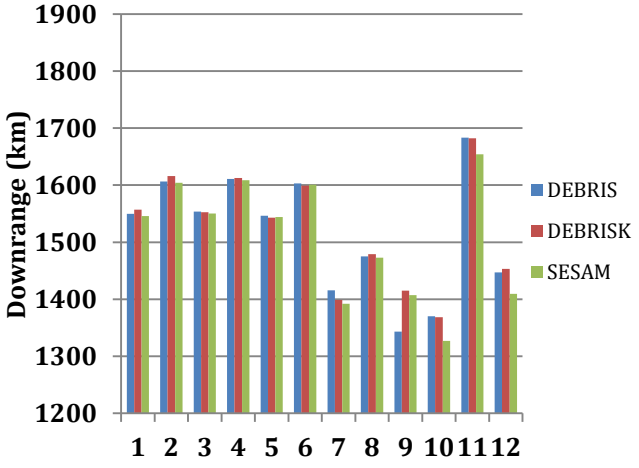

Figure 19: Downrange in km of the Integration cases

As we can see on Figure 13 to Figure ***19***, we obtain a good agreement on the results provided by the different tools for the Integration cases.
Considering the non-demising test cases, only cases 1, 3 and 7 reach the melting temperature (see Figure 14). For case 1, there is no ablation in SAM computation using SAM baseline and heating, as the heat flux computed is too low. For case 3, there is no ablation in the DEBRIS computation, as the maximum temperature of the object is 3° below the melting temperature. Also, for case 7, the ablation rate is higher for SAM computations as they are considering a randomly tumbling plate, while other tools consider a plate tumbling around the major axis.
Considering the demising test cases, we can see in Figure 15, that only the SAM computations using the SAM baseline and heating of case 9, is not 100% demised, as the heat flux is lower compared to the other tools. This explains why in Figure 13, the duration of the re-entry of case 9 computed with SAM is considerably longer.
The differences observed for cases 9 to 12, shown in Figure 17 and Figure ***18***, are due to the fact that the ablation and aerodynamics are not coupled the same way in the tools (e.g. in Debrisk both mass loss and diminution of the surface area are taken into account, while in SAM only the mass loss is accounted for. In DEBRIS the aerodynamic surface diminution is accounted for, while the mass remains constant).

3. CONCLUSIONS

A large set of comparison data for the verification process of spacecraft demise codes has been constructed thanks to the spacecraft demise workshop initiative.
All the data presented in this paper are freely available on the dedicated website of the Spacecraft Demise Workshop: http://scdw.rtech.fr.
Regarding the aerothermodynamics test cases a good agreement has been found between the high fidelity codes (CFD and DSMC). The simplified methods require improvement in the modelling of the pressure and heat flux distributions. It is clear that none of the simplified methods can ever predict complex flow features such as shock-wave boundary layer interaction, shock impingements etc. but the current work demonstrates that the current methods are over-simplified and improvements are necessary. The current study also provides indications of the dispersions in heating rates and aerodynamic coefficients that could be taken into account in a statistical approach [8].
A good agreement between the different contributions of the integrated test cases has been obtained.

4. OUTLOOK

It is foreseen to complement the test cases in different fields, such as ablation, material uncertainties, and flight mechanics. A statistical test case will be proposed that defines not only the nominal parameters, but as well the uncertainties. The outcome of the contribution to this statistical test case will be the probability density functions of parameters like demise altitude and impact energy.

5. ACKNOWLEDGEMENT

The authors would like to thank all participants for their excellent contributions to the first spacecraft demise workshop.

6. REFERENCES

1. Beck J., Merrifield J., Holbrough I., Markelov G. and Molina R.(2015).*Application of the SAM Destructive re-entry Code to the Spacecraft Demise Thermodynamics and Integration Test Cases*. Proc. of the 8th European Symposium on Aerothermodynamics for Space Vehicle

2. Parigini C., Pontijas Fuentes I., Haya Ramos R., Bonetti D. and Cornara S.(2015).*DEBRIS Tool and its Use in Mission Analysis Activities*. Proceedings of the 8th European Symposium on Aerothermodynamics for Space Vehicle

3. Omaly P. and Spel M. (2012). *DEBRISK, a Tool for Re-Entry Risk Analysis,* Proceedings of the Fifth IAASS Conference A Safer Space for Safer World

4. Martin C., Brandmueller C., Bunte K., Cheese J., Fritsche B., Klinkrad H. Lips T. and Sanchez N. (2005). *A Debris Risk Assessment Tool Supporting Mitigation Guidelines*, Proceedings of the Fourth European Conference on Space Debris

5. Couchman B. and Haynes M. (2015). *Navier-Stockes Computations for Hollow Cylinders and Cubes Relevants for Satellite Debris*, Proceedings of the 8th European Symposium on Aerothermodynamics for Space Vehicle

6. Annaloro J., Omaly P., Rivola V. and Spel M. (2015). *Elaboration of a New Spacecraft-oriented Tool: PAMPERO*, Proceedings of the 8th European Symposium on Aerothermodynamics for Space Vehicle

7. Fertig M. (2015). *Investigation of Heatflux Modification by Magnetohydrodynamic Interaction Employing the DLR CFD Code TAU*, Proceedings of the 8th European Symposium on Aerothermodynamics for Space Vehicle

8. Plazolles B., Spel M., Rivola V. and El Baz D. (2015). *Monte-Carlo Analysis of Object Reentry in Earth's Atmosphere Based on Taguchi Method*, Proceedings of the 8th European Symposium on Aerothermodynamics for Space Vehicle